Proton-Proton Scattering from 1.4 to 2.4 Mev*

DAVID J. KNECHT, S. MESSELT,† E. D. BERNERS,‡ AND L. C. NORTHCLIFFE§
University of Wisconsin, Madison, Wisconsin
(Received November 17, 1958)

Differential cross sections for the scattering of protons by protons have been measured at energies of 1.397, 1.855, and 2.425 Mev over an angular range from 12° to 90° in the center-of-mass system. Total uncertainties vary from about ±0.1% at large angles to ±0.3% at the smallest angles. A thorough investigation of sources of error has yielded cross-section values in disagreement with previously published values. A simple phase-shift analysis has been made. Without the inclusion of vacuum polarization contributions, a satisfactory fit is not obtained with only S-wave and effective nuclear P-wave phase shifts. With their inclusion, the data are fitted well by pure S-wave nuclear scattering. An upper limit on the magnitude of the effective nuclear P-wave phase shift is estimated at about 0.02° at these energies.

INTRODUCTION

THE analysis[1] of early proton-proton scattering experiments at low energies indicated the presence of a strong nuclear S-wave interaction and the absence of appreciable higher phase shifts. The experiment of Worthington, McGruer, and Findley[2] was done with greater accuracy and showed up small anomalies which were interpreted in the analysis of Hall and Powell[3] as contributions arising from small, negative, effective P-wave phase shifts.

Since the uncertainties of the WMF experiment were not much smaller than the observed anomalies, the present work was begun as an attempt to verify the results of WMF with a further reduction of experimental error and the incorporation of additional check work suggested by them. While preliminary results agreed with those of WMF, they also revealed serious discrepancies between cross sections measured with different slit systems. Subsequent theoretical work[4] and a re-analysis[5] of the WMF data indicated that satisfactory fits to the data were indeed not possible without the inclusion of large split P-wave phase shifts. These circumstances led to the measurements and the investigation of errors reported here.

EQUIPMENT

The scattering chamber, shown in Fig. 1, was originally constructed by WMF; additions and modifications to the chamber and associated equipment

were made for the present work. The chamber body is a heavy aluminum cylinder, 36 inches in diameter and 10 inches high, mounted on a solid aluminum baseplate 4 inches thick, and having an aluminum lid 2 inches thick.

The incident beam is collimated by a tube which extends into the chamber to within about 10 cm of the target volume and which contains two $1\frac{1}{2}$-mm circular defining apertures, A_1 and A_3, spaced 1 meter apart, with an antiscattering baffle, A_2, located between them. No foils are used between the accelerator and the target volume.

The unscattered beam is collected on a large Faraday cup recessed at the rear of the chamber in an evacuated housing, which is separated from the chamber by a thin nickel window. Electric and magnetic fields are provided at the cup opening for electron suppression.

The scattered particle analyzer and detector are mounted on a precision angle wheel which is constrained vertically and horizontally by ball bearings at its rim. It is rotated by a friction drive operating through a rotating seal in the baseplate. The scattered particle detector (data counter) is a proportional counter with a Mylar end window. Flexible gas and electrical leads enter through a center well in the baseplate. The analyzer consists of a rear slit or detector aperture, which is a rectangular opening to limit the counter window area, and a front slit, which limits the length along the beam viewed by the detector. The target volume thus defined by the collimator and analyzer has the shape of a truncated cone. Three sets of front and rear slits, made of stellite and having widths of 1, 2, and 4 mm, may be independently selected by use of slit-changer rods operating through seals in the lid. Each rear slit has a height 5.1 times its width.

The scattering angle defined by the analyzer axis is read by comparing the graduated scale of the angle wheel with either of two quartz-fiber index markers with the aid of microscopes mounted in the lid. An antiscattering shield is arranged to keep itself positioned between the front slit and the last capillary opening. A retractable lithium target at the center of the chamber is available for energy calibration.

[1] Breit, Thaxton, and Eisenbud, Phys. Rev. **55**, 1018 (1939).
[2] Worthington, McGruer, and Findley, Phys. Rev. **90**, 899 (1953). Referred to as WMF in text. Further details are found in H. R. Worthington, Ph.D. thesis, University of Wisconsin, 1952 (unpublished); J. N. McGruer, Ph.D. thesis, University of Wisconsin, 1951 (unpublished); and D. E. Findley, Ph.D. thesis, University of Wisconsin, 1951 (unpublished).
[3] H. H. Hall and J. L. Powell, Phys. Rev. **90**, 912 (1953). Details of the analysis are found in H. H. Hall, Ph.D. thesis, University of Wisconsin, 1952 (unpublished).
[4] Loyal Durand, III, Phys. Rev. **108**, 1597 (1957).
[5] M. deWit and L. Durand, III, Phys. Rev. **111**, 1597 (1958).

A second proportional counter located in the lid directly above the center of the chamber is used to monitor contamination. This counter views the target volume at a scattering angle of 90°, where protons scattered from hydrogen have insufficient energy to penetrate the counter window.

The gas supply system consists of commercial hydrogen cylinders, a pressure regulating valve, a catalytic purifier, and a nickel-leak purifier. In the nickel-leak purifier, gas enters a 50-foot coil of thin-wall nickel tubing, which is heated by conduction; the gas is purified by diffusion through the hot tubing wall into a region connected to the chamber. The gas inside the tubing is flushed slowly to prevent the accumulation of contaminants. Gas from the chamber flows out through the collimating tube in which there are three capillary constrictions, one associated with each collimating aperture or baffle. The pressure regions so defined have separate vacuum pumping systems and form a differentially pumped transition from chamber pressure to a high vacuum. Chamber gas is flushed in this way at the rate of 18 atmospheric liters per hour.

The chamber pressure is measured by use of a glass manometer filled with Octoil-S. The heights of the two menisci are measured by comparison with division marks of a scale placed between the manometer arms. A cathetometer with two travelling telescopes to view the menisci and the scale is used to interpolate between scale divisions. A second manometer is used as an element of a pressure stabilizing system. A light source and a photosensitive crystal are mounted at each meniscus; the oil column below the meniscus acts as a cylindrical lens to focus on the crystal a line image which is terminated by the meniscus. Resistance changes of the crystals caused by movement of the menisci are used as an error signal to vary the power supplied to a small heater coil concealed in the capillary nearest the chamber center; the resulting changes in gas temperature vary the mass rate at which gas flows out of the chamber.

The temperature of the target gas is measured with accurately calibrated mercury thermometers which are inserted in small oil-filled wells in the lid and baseplate. Temperature stabilization is achieved by sensitive thermostatic control of room temperature.

A beam-control system is used to stabilize further the direction of the incident beam in the chamber. A vertical slit, $\frac{1}{4}$ mm in width and centered on the collimator axis, is formed by two separately insulated jaws in the collector cup; almost all of the unscattered beam falls on these jaws and the current from them passes through a well-insulated reflecting-type galvanometer movement, shunted in such a way as to make its deflection proportional to the difference in currents from the two jaws. The deflection is read by photocells mounted at the scale position to provide an error signal which varies the current in a beam-deflecting magnet
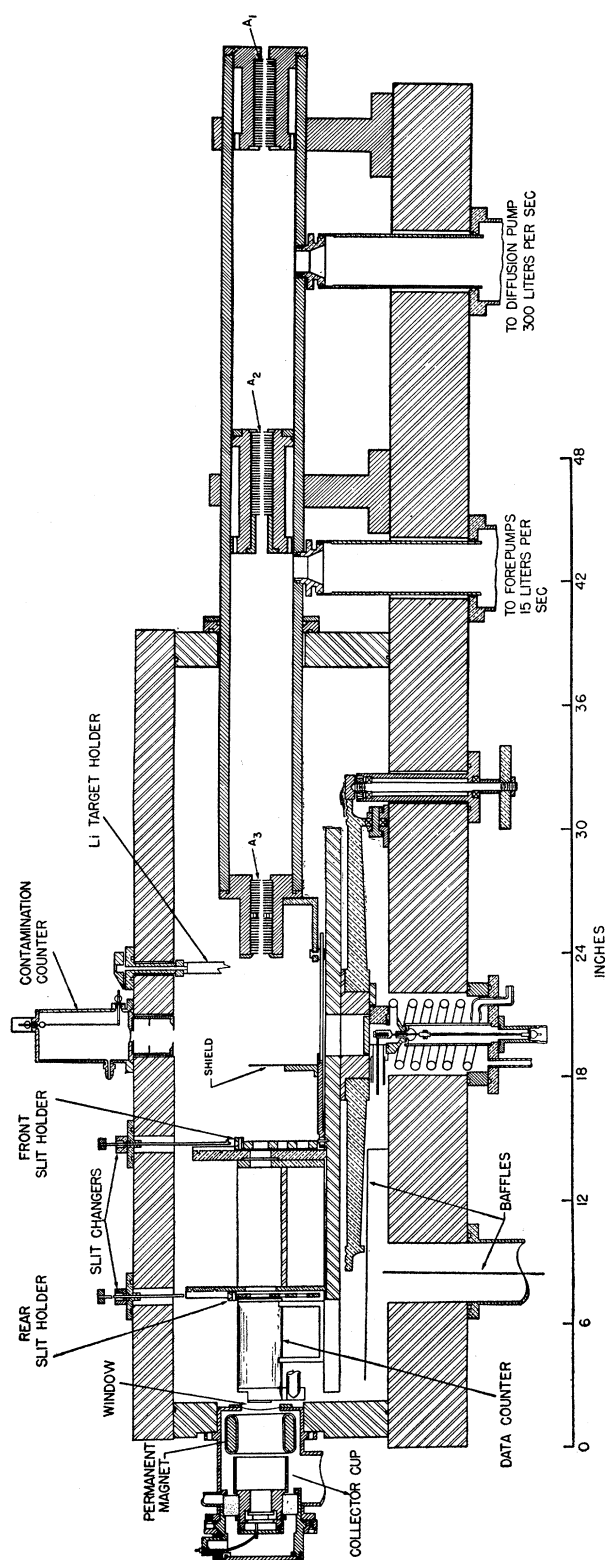
FIG. 1. Sectional view of the scattering chamber with the scattering angle set at zero.

at the first collimating aperture; the beam is thus kept centered on the slit.

The current collected on the slit jaws, as well as on other portions of the collector cup, is passed through a current integrating circuit, which consists of a 4-microfarad polystyrene condenser, a network to charge the condenser to a known potential of about 10 volts, and a sensitive null-detecting dc amplifier. The condenser, initially charged, is discharged completely by the beam current, at which time the null detector terminates the run by simultaneously disconnecting the beam-current and counting circuits.

Pulses from the data counter are amplified, clipped with a 1-μsec delay line, and fed to three discriminator-scaler circuits, termed the A, B, and C scalers. They are also fed to a 10-channel pulse-height analyzer for detailed study of the pulse spectrum. Pulses from the fixed 90-degree counter are amplified, RC-clipped, and fed to two discriminator-scaler circuits. Discriminator levels are set with a precision pulse generator.

The incident proton beam is obtained from an electrostatic accelerator. Particles other than protons are excluded by magnetic deflection and the proton energy is defined and measured with a cylindrical electrostatic analyzer with a slit system adjusted to give an energy spectrum 0.1% wide at half-maximum.

PROCEDURE

To measure the cross section at each angle, runs were made in pairs, with the counter set alternately at positions to the right and to the left of the beam, until the desired number (usually 1 million) of counts had been obtained. Data usually recorded for each run were the A-, B-, and C-scaler and 10-channel yields, scattering angle, slit width, time of day, run duration, contamination yield, and integrator end-point readings. A continuous log was kept of the chamber pressure and the temperatures of the lid, baseplate, oil, integrating condenser, and room air. Observation and adjustment were made as often as necessary of beam control operation, integrator charging voltage, null detector zero, incident beam energy, normal pulse height in both counters, background levels, and counter voltage and pressure. Detection of malfunctioning equipment was aided by the predictability and interdependence of the observed data.

The angular range covered by each slit system was extended to provide four points measured by two slit systems and one point measured by all three.

The final values for cross sections at 1.855 Mev result from seven complete or partial angular distribution measurements. At 1.397 and at 2.425 Mev a single measurement was made.

The energy value for each distribution was deduced from measurements of the $Li^7(p,n)Be^7$ threshold energy. Eight such determinations were made during the course of final angular distribution measurements.

CALCULATION OF THE EXPERIMENTAL CROSS SECTIONS

The cross section in the laboratory system, σ, is related to the yield of scattered particles per run, Y, by the expression

$$\sigma = Y \sin\theta / nNG, \tag{1}$$

where θ is the laboratory scattering angle, n is the total number of incident protons, N is the target proton density, and G is a geometrical factor given in terms of the front-slit half-width b_1, rear-slit half-width b_2, rear-slit height l, spacing h between slits, and the distance R_0 of the rear slit from the target volume by the approximation

$$G \simeq 4b_1b_2l/R_0h. \tag{2}$$

The number of incident protons n, integrated by allowing them to discharge a condenser of capacitance C from an initial voltage $-V$ to zero, is given by

$$n = CV/e \tag{3}$$

where e is the electronic charge. The density N is given by

$$N = 2L_0(t_0/t)(\rho g H / A_0), \tag{4}$$

where L_0 is Loschmidt's number defined for temperature t_0 (0°C), and a pressure of one standard atmosphere, A_0. The other quantities are the target gas temperature t, the manometer oil density ρ, the gravitational acceleration in the laboratory g, and the height of the manometer oil column H. The cross section in the center-of-mass system is given approximately by

$$P \simeq \sigma / (4 \cos\theta). \tag{5}$$

and the center-of-mass scattering angle, Θ, is approximately

$$\Theta \simeq 2\theta. \tag{6}$$

The center-of-mass cross sections were calculated from the resulting expression:

$$P \simeq \left[\frac{etR_0hA_0}{32CVL_0t_0\rho gHb_1b_2l} \right] Y \tan\theta. \tag{7}$$

The bracketed factor was assumed to be constant for each set of analyzer slits. Small deviations from its constant value caused by fluctuations and inaccurate approximations were taken into account by applying small percentage corrections to the cross sections thus calculated. In the same way corrections were applied for spurious additions to and losses from the yield.

CORRECTIONS

In the measurement of scattering cross sections to an accuracy of a few parts per thousand, many sources of error become appreciable; in the present work the major effort was directed toward the reduction, control, and calculation of these errors. The following

paragraphs describe the experimental methods employed to reduce and control recognized errors and the calculated corrections applied to the experimental cross sections. Those corrections which exhibit an inherent angular dependence and which, if ignored or made incorrectly, might confuse the interpretation of the angular distribution data, are shown in Fig. 2.

Temperature

The temperature of the target gas was found by averaging the lid and baseplate thermometer readings. Thermometer scales were corrected by assuming a linear calibration between the ice and sodium sulfate points. The temperature rise at the target volume caused by absorption of energy from the beam was calculated. Temperature gradients within the chamber were minimized by the large thermal conductivity and

mass of the chamber and by control of room temperature. The uncertainty estimated in the temperature determination was $\pm 0.02\%$.

Pressure

The determination of pressure involves the reading of the oil column height. The total uncertainty resulting from various scale and screw calibrations, telescope alignments, and resolution of the optics was estimated at $\pm 0.02\%$. The density of the manometer oil at several temperatures was measured by the standard pycnometer method; the temperature of the oil was recorded during the taking of data and used with the observed coefficient of thermal expansion to make a density correction. The uncertainty in density was estimated at $\pm 0.02\%$. The effects of surface tension at the oil menisci, pressure gradients, and deviations from ideal gas behavior were considered and found negligible. The pressure-control system stabilized pressure to within 0.01% over long periods of time and drifts contributed no additional uncertainty.

Flux Integration

The accuracy of incident flux integration reflects errors in both the collection of particles and the measurement of total charge. The loss of particles from the beam by scattering in the chamber gas and the collector cup window is minimized by the large diameter of the cup and window. A correction for this loss was calculated by integration of the Rutherford scattering formula; its uncertainty, estimated at $\pm 20\%$, arises largely from an uncertainty in the window thickness. Errors caused by secondary electrons leaving the cup or window were made negligible by the combination of magnetic and electric suppression fields placed between these two objects. The error caused by the collection of ions produced by bombardment of gas in the region of the collector cup was made negligible by maintaining a sufficiently good vacuum in the cup housing. Electrical leakage was made negligible by the provision of very good electrical insulation and the maintenance of low humidity in the laboratory.

The current integrator circuit built by WMF is capable of 0.01% precision; provision is made to measure at the end of each run the residual charge on the integrating condenser and the total charge drawn as grid current by the null detector. The initial voltage of the condenser is measured by comparison with a standard cell. An over-all calibration of the integrator was made by the current-time method with an accuracy of $\pm 0.04\%$ to find the value of the total charge collected per run. The calibration was made with the integrator connected and operating as in an ordinary yield measurement except that the charge was supplied by a current source connected to the cup; several possible sources of error were thus eliminated without special effort. A small error arises from the variation of the
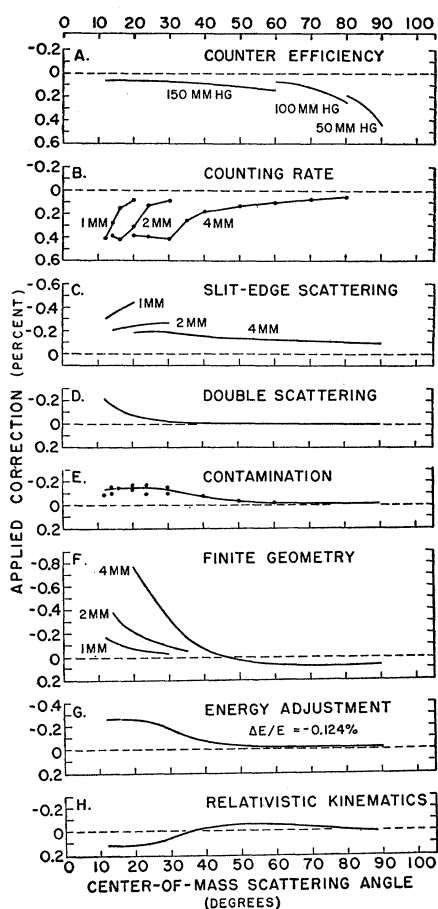
FIG. 2. Corrections and adjustments applied to the experimental data at 1.855 Mev plotted as percentages of the total value of the differential cross section. In A the labels refer to the pressure of the argon-CO_2 counter gas. In B, C, and F the labels refer to the analyzer slit width. In B and E individual points represent corrections applied in a typical distribution measurement. In E the solid curve is calculated to fit the experimental points with the assumption of a constant percentage contamination of air. In G the assumed energy difference is that which applied to most of the measurements at 1.855 Mev.

integrator capacitance with temperature; the co-efficient determined by WMF was used to make a correction.

Detection Efficiency

Among the errors affecting the observed yields is the counter-efficiency error which results from the scattering of particles out of the active volume of the counter by the window and the counter gas. The counter was operated at a pressure low enough that a normal proton would pass entirely through the active counter volume, losing only part of its energy; low pulses therefore resulted almost entirely from protons scattered in the window or the counter gas, and a study of the low-pulse spectrum could be used to correct for losses from this cause. The A, B, and C scalers were set with thresholds at 8, 16, and 50 volts, respectively, while the normal pulse height was main-tained at 40 volts. The yield in the 8–16 volt channel, termed the A-B difference, was above background and was available for each run as an estimate of the low-pulse component of the yield. From a knowledge of the window thickness and composition, the gas pressure and composition, and the counter dimensions, a calcu-lation could be made of the number of protons expected to miss entirely the active counter volume. Inter-polation then gave an estimate of the number of pulses expected in the 0–8 volt channel. The sum of these three groups constituted the total loss since the basic yield was taken from the B scaler. In a detailed study during preliminary work, the total loss was found to be related to the A-B difference by a constant factor for the counter conditions normally utilized. A semi-empirical formula was also found which accurately predicted the A-B difference from the counter condi-tions and particle energy. The observed and calculated A-B differences were used to calculate a counter-efficiency correction [Fig. 2(A)] for each measured yield. The uncertainty in the correction was estimated at ±10%.

An additional error in the yield was caused by the finite resolving time of the scaling circuits. A careful study of yield as a function of counting rate gave the most reliable value for the resolving time of the B scaler; this value was multiplied by the average counting rate to find a counting-rate correction [Fig. 2(B)] for each run. The correction was estimated to be uncertain to ±10% and counting rates were usually limited to 2000 counts per second to avoid corrections in excess of 0.2%. The difference in resolving times for the A and B scalers was also taken into account in computing A-B differences.

Slit-Edge Scattering

A slit-edge scattering error arises from the partial transparency of the slit edges to scattered protons; although the entire thickness of a slit jaw is sufficient

to stop a proton of full energy, it is possible for a proton striking the front face or edge surface to emerge after a short path in the material of the jaw having lost only a fraction of its energy. Thus a certain number of protons, having first been scattered from some point in the beam in such a way that they should not be counted, suffer a collision with a slit edge which directs them into the detector where they are counted.

This process gives rise to protons of abnormally low energy. Since a normal proton passes entirely through the counter, losing only a fraction of its energy, a proton of abnormally low energy will produce a higher pulse than normal. Thus, although pulses caused by slit-scattered protons are included in the B-scaler yield, they are characterized by excessive height. Data obtained with the C scaler, the threshold of which was set 25% above normal pulse height, were used as the experimental basis for a correction for this effect. Since high pulses can also be caused by the accidental superposition of normal pulses, it was necessary first to remove this contribution from the C-scaler yield. The maximum time interval by which two pulses could be separated and still produce a pulse high enough to register in the C scaler was found by meas-uring the C-scaler yield as a function of counting rate; this time interval multiplied by the counting rate and by the B-scaler yield gave for each run the number of pulses in the C-scaler yield which could be attributed to superposition. The remainder were assumed to represent low-energy protons. The energy intervals over which the B and C scalers could count were found from a measured curve of pulse height as a function of energy. Under the assumption of a uniform distribution in energy of the slit-scattered protons, the slit-edge contribution to the B-scaler yield was inferred from the corresponding C-scaler yield by multiplying by the ratio of these energy ranges.

A theoretical estimate of the slit-edge contribution to the yield, based on the model of Courant,[6] was also made. Courant's results were applicable directly to scattering by the rear slit edges and were re-evaluated with the aid of analytic and graphical integration to make them applicable to scattering by the front slit edges. A detailed consideration of the geometry involved in the illumination by scattered protons of the various slit edges and in the acceptance by the counter of slit-scattered protons, as well as a considera-tion of counter operating conditions, made possible the conversion of these results into an estimate of the slit-edge contribution to the B-scaler yield. The experi-mental and theoretical estimates were substantially in agreement; the former were somewhat larger and somewhat scattered. The correction applied to the data [Fig. 2(C)] retained the angular dependence of the theoretical estimate, which was arbitrarily adjusted in magnitude to conform to the experimental data.

---
[6] E. D. Courant, Rev. Sci. Instr. **22**, 1003 (1951).

The possibility of a low-energy component in the incident beam was not experimentally investigated; such protons, scattered normally, would also produce high pulses indistinguishable from slit-scattered proton pulses and would cause a spurious addition to the yield because of the energy dependence of the cross section. The two errors are not quantitatively the same, however, and the possibility of confusing them to some extent necessitates the assignment of an uncertainty of $\pm 33\%$ in the slit-edge-scattering correction.

Double Scattering

Processes in which a proton from the incident beam undergoes two scattering collisions in the chamber gas lead to an appreciable error in the measured yields. Those in which particles are lost from the scattered proton beam passing through the analyzer are generally compensated for very well by those which add spurious protons unless the geometry is such as to interfere with such processes. The present chamber was designed to take full advantage of such compensation. Worthington has given formulas for the net error to be expected from incomplete compensation. These have been used to make a double-scattering correction to the data [Fig. 2(D)]; the estimated uncertainty is $\pm 50\%$.

Contamination

The use of the nickel-leak purifier and the replacement of some chamber parts with components of lower vapor pressure greatly reduced the contamination. However, since the scattering at small angles from heavier elements is much stronger than from hydrogen, the presence of a small percentage of contaminant in the chamber gas produces an error of much larger percentage in the yield of scattered protons. The yield in the 90-degree counter was used to estimate the contaminant contribution to the B-scaler yield for each run on the assumption that the contaminant was air. Differential cross sections for oxygen and nitrogen were obtained from published data or from measurements made with the chamber filled with these gases. The assigned uncertainty of $\pm 25\%$ in the correction thus calculated [Fig. 2(E)] arises mainly from uncertainty as to the composition of the contaminant and from the statistical uncertainty of the yield in the 90-degree counter.

Contamination by deuterium was a special case in that it was not removed by the nickel-leak purifier and was not detectable by the 90-degree counter. A correction was calculated from published cross-section values and the assumption that it was present in its natural abundance.

Geometry

A variety of errors arise in connection with the geometrical arrangement of the collimator and the scattered-particle analyzer. The requirements of angular

accuracy and alignment of parts were considered by WMF in the design of the chamber and were re-investigated during the present work.

The alignment of the collimating apertures, the center of rotation, the front and rear analyzing slits, and the slit in the collector cup was checked at the zero of the angle wheel by using a lens placed behind the opened collector cup housing to project real images of these objects. The relative positions of the various images were then determined by a combination of travelling cross-hair, microscope, and Michelson interferometer, and the corresponding positions of the objects were calculated.

The observed alignment was precise enough to insure a negligible error in the average yield for equal numbers of measurements made with the counter placed to the right and to the left of the beam if the position of the beam did not change. In preliminary work it was found possible to effect a 1% change in yield at the smallest angles by deflecting the beam through the range of positions allowed by the collimator without loss of intensity; the possibility that fluctuations approaching this size might occur between yield measurements made to the right and to the left of the beam led to an appreciable uncertainty in the average yield when relatively few measurements were included. The beam-control system was introduced to eliminate this uncertainty.

The slit dimensions, b_1, b_2, and l, were measured with the use of an accurately calibrated dividing engine screw and a microscope. The distances, R_0 and h, were similarly measured with the additional aid of graduated bars placed between the slit faces and the center of rotation. The total uncertainties in the G-factors thus determined were $\pm 0.14\%$, $\pm 0.08\%$, and $\pm 0.04\%$, for the 1-, 2-, and 4-mm slits, respectively.

A precise expression for the G-factor, which is approximated by Eq. (2), involves an expansion in the successive derivatives of the cross section, where the coefficients involve ratios of analyzer and collimator dimensions and spacings. Approximations previously used were found not to be sufficiently accurate, and a new expression, derived by Silverstein,[7] was used to calculate a correction for finite analyzer and collimator geometry [Fig. 2(F)]. The derivatives needed were found from analytic differentiation of the expression for the pure S-wave cross section with the experimental value of the phase shift, and the entire calculation was programmed for machine computation.

[7] E. A. Silverstein, Nuclear Instr. (to be published). The expression used in the present work is (if ρ is the radius of the collimator apertures)

$$G = [4b_1b_2l/R_0h][1 + (-b_1^2/2h^2 - b_2^2/2h^2 - 3l^2/24R_0^2 + b_2^2 \cot^2\theta/3R_0^2$$
$$+ \rho^2 \csc^2\theta/4R_0^2 - 3\rho^2/8R_0^2) + (l^2/24R_0^2 - b_2^2/3R_0h$$
$$+ \rho^2/8R_0^2)(\cot\theta)(\sigma'/\sigma) + (b_1^2/6h^2 + b_2^2/6h^2)(\sigma''/\sigma)$$
$$+ (-b_2^4/30R_0h^3 - b_1^2b_2^2/18R_0h^3 + b_1^2l^2/144R_0^2h^2$$
$$+ b_2^2l^2/144R_0^2h^2 + \rho^2b_1^2/24R_0^2h^2 + \rho^2b_2^2/24R_0^2h^2)(\cot\theta)(\sigma'''/\sigma)$$
$$+ (b_1^4/120h^4 + b_2^4/120h^4 + b_1^2b_2^2/36h^4)(\sigma''''/\sigma)].$$

TABLE I. Values of the cross section at 1.855 Mev.

Center-of-mass scattering angle Θ	Experimental value of the center-of-mass cross section P_e (barns)	S- plus P-wave (vac. pol. included) $K_0 = 44.246°$ $K_1 = -0.011°$		Pure S-wave (vac. pol. included) $K_0 = 44.259°$ $K_1 = 0$		S- plus P-wave (vac. pol. omitted) $K_0 = 44.274°$ $K_1 = -0.040°$	
		P_f (barns)	$(P_e-P_f)/P_f$	P_f (barns)	$(P_e-P_f)/P_f$	P_f (barns)	$(P_e-P_f)/P_f$
12°	11.179 ±0.30%	11.193	−0.12%	11.189	−0.09%	11.143	+0.32%
14°	5.8277 ±0.26%	5.8267	+0.02%	5.8239	+0.07%	5.8007	+0.46%
16°	3.2901 ±0.25%	3.2927	−0.08%	3.2906	−0.01%	3.2783	+0.36%
20°	1.2658 ±0.23%	1.2676	−0.15%	1.2663	−0.04%	1.2629	+0.23%
24°	0.59900±0.22%	0.59959	−0.10%	0.59876	+0.04%	0.59812	+0.15%
30°	0.27800±0.19%	0.27838	−0.14%	0.27792	+0.03%	0.27835	−0.13%
35°	0.19689±0.18%	0.19680	+0.05%	0.19652	+0.19%	0.19703	−0.07%
40°	0.16757±0.13%	0.16751	+0.03%	0.16735	+0.13%	0.16777	−0.12%
50°	0.15637±0.11%	0.15624	+0.08%	0.15621	+0.10%	0.15638	0.00%
60°	0.15999±0.11%	0.15980	+0.12%	0.15983	+0.10%	0.15980	+0.12%
70°	0.16435±0.11%	0.16436	0.00%	0.16443	−0.05%	0.16426	+0.05%
80°	0.16733±0.11%	0.16734	−0.01%	0.16743	−0.06%	0.16720	+0.08%
90°	0.16781±0.14%	0.16835	−0.32%	0.16845	−0.38%	0.16819	−0.23%

Energy Determination

The calculation of the energy was based on measurements of the $Li^7(p,n)Be^7$ reaction threshold at 1.8811 Mev.[8] The lithium fluoride target, mounted at the center of the chamber, was evaporated onto a thin nickel foil to allow integration of the incident flux in the usual way. The deviation from linearity of the curve of energy as a function of plate voltage was incorporated in making a relativistically correct calibration of the cylindrical electrostatic analyzer. The energy loss of the incident beam in the chamber gas ahead of the target volume was found at the threshold energy by measuring the threshold with the chamber both filled and evacuated and was extrapolated to other energies with the aid of published values of the stopping power. The total uncertainty in the energy was estimated at ±0.09% and includes uncertainties in the calibration measurement, the loss in the gas, and the accepted value of the threshold energy.

ADJUSTMENTS

Two additional adjustments of the data were made in a manner similar to that of applying corrections in order to afford greater convenience in the tabulation and analysis of results. Each has a characteristic angular dependence. Neither adds an appreciable uncertainty.

Energy Adjustment

It was not always possible to know accurately, in advance, the energy of an angular distribution, and small deviations from the nominal energy were encountered. In order to compare and average these measurements, all cross-section values were adjusted to the nominal energy by using a calculated value of the derivative of the cross section with respect to

energy. The expression for the pure S-wave cross section was differentiated analytically and programmed for machine computation; experimental values of the phase shift and its derivative with respect to energy were used. The angular dependence exhibited by this adjustment [Fig. 2(G)] is the same as that which would be introduced into the angular distribution by an incorrect determination of the energy.

Relativistic Kinematics

The nonrelativistic approximations given by Eqs. (5) and (6) are not sufficiently accurate for the present purpose; the relativistically correct relations, which are also simple, permit the calculation of cross sections at center-of-mass angles which are slightly different from twice the measured laboratory angles. However, it is more convenient to have cross sections quoted for exactly twice the laboratory angle; therefore, the previously computed derivatives with respect to angle were used to adjust all cross-section values to make them relativistically correct at exactly the nominal center-of-mass angle. The curve of Fig. 2(H) shows

TABLE II. Values of the cross section at 1.397 Mev.

Center-of-mass scattering angle Θ	Experimental value of the center-of-mass cross section P_e (barns)	Calculated value S- plus P-wave (vac. pol. included) $K_0 = 39.208°$ $K_1 = -0.017°$	
		P_f (barns)	$(P_e-P_f)/P_f$
12°	20.136 ±0.34%	20.128	+0.04%
14°	10.553 ±0.32%	10.515	+0.36%
16°	5.9603 ±0.27%	5.9502	+0.17%
20°	2.2746 ±0.26%	2.2687	+0.26%
24°	1.0341 ±0.23%	1.0327	+0.14%
30°	0.42068±0.20%	0.42061	+0.02%
35°	0.25567±0.17%	0.25609	−0.16%
40°	0.19139±0.16%	0.19150	−0.06%
50°	0.15736±0.14%	0.15716	+0.13%
60°	0.15615±0.14%	0.15624	−0.05%
70°	0.16050±0.14%	0.16047	+0.02%

[8] Jones, Douglas, McEllistrem, and Richards, Phys. Rev. 94, 947 (1954).

the total difference between the cross-section values thus adjusted and those calculated by use of Eq. (5).

RESULTS

Final values of the cross sections are given in Tables I, II, and III. At all energies the values obtained with different slit systems have been averaged, and at 1.855 Mev the values from the various angular distribution measurements have been averaged. In averaging, no attempt was made to weight the various values according to their uncertainties; at a given angle these did not differ greatly.

The uncertainty listed for each point is the total of all recognized uncertainties, most of which have been discussed, compounded quadratically. A separation into systematic and nonsystematic uncertainty has not been made since some contributions exhibit characteristics of each; further, absolute value is of no less importance than relative value in the analysis to follow, and nonsystematic uncertainty may be inferred to some extent by the scatter of the points.

The present data are not in good agreement with the data of WMF, differing by nearly 1% at small angles. The differences have generally been explained by newly discovered errors and revisions in applied corrections. No significant discrepancies are now found between cross-section values measured with different slit systems. The estimated uncertainty in each of the present cross-section values has been reduced to about half of that in the previous values.

ANALYSIS

In attempting to reduce cross-section data to a set of phase shifts it is reasonable to try the simplest possibilities first; therefore it was tentatively assumed that all phase shifts for states of $L>1$ were zero and that the triplet P-wave phase shifts were independent of J. The scattering amplitudes given by Breit and

Hull[9] were used to find the Coulomb and nuclear S- and P-wave contributions to the cross section, P_M, ΔP_0, and ΔP_1, respectively, and the vacuum polarization contributions, ΔP_{vp}, were taken from the numerical values computed by Durand.[10] The angular dependence of small contributions to the cross section at 1.855 Mev is shown in Fig. 3. The cross section in the center-of-mass system is given by

$$P = P_M + \Delta P_0 + \Delta P_1 + \Delta P_{vp}, \qquad (8)$$

where

$$P_M = \frac{\eta^2}{4k^2}\left[\frac{1}{s^4} + \frac{1}{c^4} - \frac{1}{s^2c^2}\cos\left(\eta\ln\frac{s^2}{c^2}\right)\right],$$

$$\Delta P_0 = \frac{\eta^2}{4k^2}\left[-\frac{2}{\eta}(X_s + X_c)\sin K_0\cos K_0\right.$$
$$\left. +\frac{2}{\eta}(Y_s + Y_c)\sin^2 K_0 + \frac{4}{\eta^2}\sin^2 K_0\right], \quad (9)$$

$$\Delta P_1 = \frac{\eta^2}{4k^2}\left[-\frac{18C}{\eta}(X_{s1} - X_{c1})\sin K_1\cos K_1\right.$$
$$\left. +\frac{18C}{\eta}(Y_{s1} - Y_{c1})\sin^2 K_1 + \frac{108C^2}{\eta^2}\sin^2 K_1\right],$$

and where the notation is as follows:

$\eta = e^2/\hbar v$,

$k^2 = M_p E/2\hbar^2$,

$E =$ particle energy (laboratory system),

$v =$ particle velocity (laboratory system),

$s = \sin\theta$,

$c = \cos\theta$,

$C = \cos\Theta = P_1(\cos\Theta)$,

$K_0 = S$-wave phase shift,

$K_1 = P$-wave phase shift (effective), (10)

$X_s = s^{-2}\cos(\eta\ln s^2)$,

$X_c = c^{-2}\cos(\eta\ln c^2)$,

$Y_s = s^{-2}\sin(\eta\ln s^2)$,

$Y_c = c^{-2}\sin(\eta\ln c^2)$,

$X_{s1} = s^{-2}\cos(\eta\ln s^2 + 2\tan^{-1}\eta)$,

$X_{c1} = c^{-2}\cos(\eta\ln c^2 + 2\tan^{-1}\eta)$,

$Y_{s1} = s^{-2}\sin(\eta\ln s^2 + 2\tan^{-1}\eta)$,

$Y_{c1} = c^{-2}\sin(\eta\ln c^2 + 2\tan^{-1}\eta)$.

The importance of calculating the particle velocity, v,

TABLE III. Values of the cross section at 2.425 Mev.

Center-of-mass scattering angle Θ	Experimental value of the center-of-mass cross section P_e (barns)	Calculated value S- plus P-wave (vac. pol. included) $K_0 = 48.273°$ $K_1 = -0.019°$ P_f (barns)	$(P_e - P_f)/P_f$
12°	6.4602 ±0.29%	6.4600	0.00%
14°	3.3622 ±0.25%	3.3622	0.00%
16°	1.9032 ±0.25%	1.9067	−0.18%
20°	0.75240±0.23%	0.75317	−0.10%
24°	0.37863±0.23%	0.37887	−0.06%
30°	0.20439±0.21%	0.20399	+0.20%
35°	0.16195±0.17%	0.16216	−0.13%
40°	0.14874±0.15%	0.14873	+0.01%
50°	0.14636±0.13%	0.14628	+0.06%
60°	0.15073±0.14%	0.15043	+0.20%
70°	0.15431±0.13%	0.15418	+0.08%
80°	0.15647±0.13%	0.15647	0.00%
90°	0.15703±0.14%	0.15723	−0.12%
100°	0.15613±0.14%	0.15647	−0.22%

[9] G. Breit and M. H. Hull, Jr., Phys. Rev. 97, 1047 (1955).
[10] Values were taken from Table II of reference 4 except for the value for 12° c.m. at 1.855 Mev, which was taken from footnote 17 of reference 5.
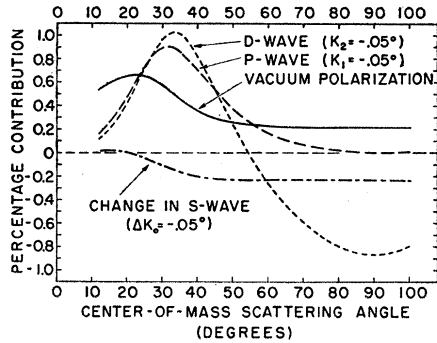
FIG. 3. Small contributions to the calculated differential cross section at 1.855 Mev plotted as percentages of the total value. Vacuum polarization contributions are from reference 4; P- and D-wave contributions are calculated for assumed values of K_1 and K_2. Also shown is the change in cross section produced by a small decrease in K_0 (for $K_0 \simeq 44.2°$).

relativistically was emphasized by Durand; relativistically correct parameters were used throughout the present analysis.

The procedure of Hall and Powell[3] was adapted to make a fit to the experimental points. A first value for the cross section, P^*, was calculated from estimated values for the phase shifts, K_0^* and K_1^*. The value of K_1^* was taken to be zero; the value of K_0^* was taken as the average of values found by solving the cross-section expression for K_0 and using the experimental data to evaluate for angles near 90° c.m. The final-fit cross section, P_f, was assumed to be given by

$$P_f = P^* + A(\partial P/\partial K_0) + B(\partial P/\partial K_1). \qquad (11)$$

The expression for the weighted sum of the squares of the deviations of the experimental values from the values of P_f was minimized by variation of the quanti-

TABLE IV. Results of phase-shift analysis.

Lab energy E (Mev)	Contributions included[a]	Method of weighting[b]	S-wave phase shift K_0	Effective P-wave phase shift K_1
1.855	S, P, V	1	44.246°	−0.011°
	S, P, V	2	44.265°	−0.002°
	S, P, V	3	44.246°	−0.008°
	S, V	1	44.259°	
	S, P	1	44.274°	−0.040°
1.397	S, P, V	1	39.208°	−0.017°
	S, P, V	2	39.191°	−0.021°
	S, P, V	3	39.198°	−0.020°
	S, V	1	39.238°	
	S, P	1	39.226°	−0.048°
2.425	S, P, V	1	48.273°	−0.019°
	S, P, V	2	48.279°	−0.017°
	S, P, V	3	48.286°	−0.016°
	S, V	1	48.294°	
	S, P	1	48.297°	−0.051°

[a] Terms included in the cross-section expression (in addition to Mott terms) are indicated by S (S-wave terms), P (P-wave terms), and V (vacuum polarization terms).
[b] The weight attached to each experimental point is indicated by method 1 (reciprocal square of the uncertainty), method 2 (number of measurements included in the average), and method 3 (equal weight at each point).

ties A and B. Equation (11) is justified if A and B turn out to be sufficiently small. The desired phase shifts are then

$$K_0 = K_0^* + A,$$
$$K_1 = B. \qquad (12)$$

The analysis was programmed for machine computation. At each energy, three such analyses were made with the weight at each angle being assigned as (1) the reciprocal square of the total uncertainty, (2) the total number of measurements included in the average, or (3) unity. The results of the three methods did not differ significantly; in subsequent analyses only the first method of weighting was employed. The data were also analyzed with the omission of the vacuum polarization contributions. Since the first analyses
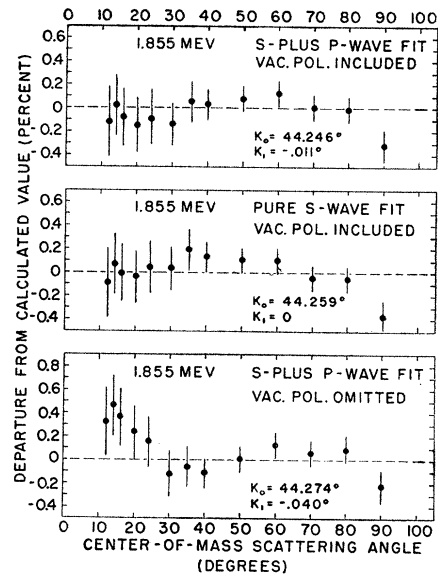
FIG. 4. Departures of the experimental data at 1.855 Mev from cross section values calculated to fit the data by a least-squares procedure.

yielded very small P-wave phase shifts, a least-squares fit by a pure S-wave cross section was also made. The phase shifts derived by these analyses are given in Table IV. Details of the fits obtained in three of the analyses at 1.855 Mev are given in Table I and Fig. 4. Details of one analysis at each of the energies 1.397 and 2.425 Mev are similarly given in Tables II and III and Fig. 5. Each of these five fits given in detail employed method 1 in weighting the data.

DISCUSSION

An estimate of the uncertainty in the P-wave phase shifts found by the analysis may be made by observing that if K_1 were 0.02° in magnitude, the maximum fractional contribution to the cross section would be 0.004 in a region where the uncertainties are 0.002; it would seem unreasonable to expect a smaller contribu-

tion to be detected. Similarly, if K_0 were changed by 0.04°, the maximum fractional change in the cross section would be 0.002 in a region where the uncertainties are 0.001.

The data at 1.855 Mev are the result of repeated measurement under somewhat varied conditions. They are fitted very well by a pure S-wave cross section. Without the inclusion of vacuum polarization contributions for $L>1$ (the vacuum polarization P-wave phase shift becomes included in K_1), the fit is not satisfactory, especially since relative uncertainties are smaller than the total absolute uncertainties shown; a significant systematic anomaly remains. It appears that its large
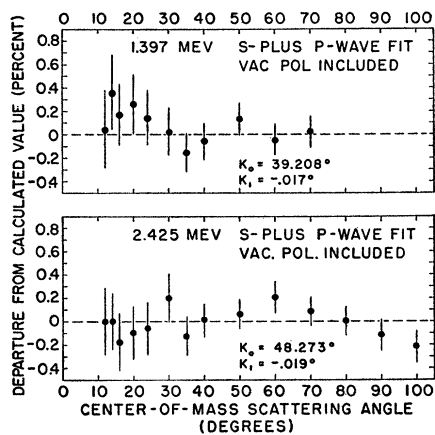
FIG. 5. Departures of the experimental data at 1.397 and 2.425 Mev from cross section values calculated to fit the data by a least-squares procedure.

contribution at small angles makes the vacuum polarization effect distinguishable from expected nuclear effects.

The distributions at 1.397 and 2.425 Mev are each the result of a single measurement, and the random scatter of the points is greater than at 1.855 Mev.

Acceptable fits give P-wave phase shifts which approach a significant magnitude, but the pure S-wave fits are not greatly inferior. The acquisition of more data at these energies will be undertaken, and the present values should be regarded as preliminary.

In general, it may be said that the present data place an upper limit of about 0.02° on the magnitude of the effective P-wave phase shift at energies from 1.4 to 2.4 Mev. The possibility of much larger split P-wave as well as D-wave phase shifts is not excluded.[11] It should be remarked that the S-wave phase shifts derived here include the effect of the vacuum polarization interaction for $L=0$, since the contributions calculated by Durand result only from states with $L>0$. Further, it should be mentioned that a new consideration of the effects of molecular electrons on the scattering has been made by Breit,[12] who has pointed out that compensation of inelastic scattering by inelastic effects on the coherent scattering is not likely to be good in this energy range. Rough calculations indicate that the net change in cross section from this effect may be as large as the experimental uncertainty in the present data.

ACKNOWLEDGMENTS

---

[11] M. H. Hull, Jr., and J. Shapiro, Phys. Rev. 109, 846 (1958).
[12] G. Breit, Phys. Rev. Letters 1, 200 (1958).